SUPPLEMENTAL INFORMATION

Supplemental Figures linked to the main manuscript

Supplemental Figure	Title	Relates to
Figure S1	Steady-state levels of TE and germline transcripts during normal and *Dnmt3L* mutant spermatogenesis	Figure 1
Figure S2	Participation of the piRNA pathway to the regulation of TEs during *Dnmt3L* mutant spermatogenesis	Figure 2
Figure S3	Gene expression and cell progression at meiosis in *Dnmt3L* mutant testes	Figures 2, 3 and 4
Figure S4	H3K9 methylation patterns and effects of *Spo11* deficiency in *Dnmt3L* mutant testes	Figures 3 and 4

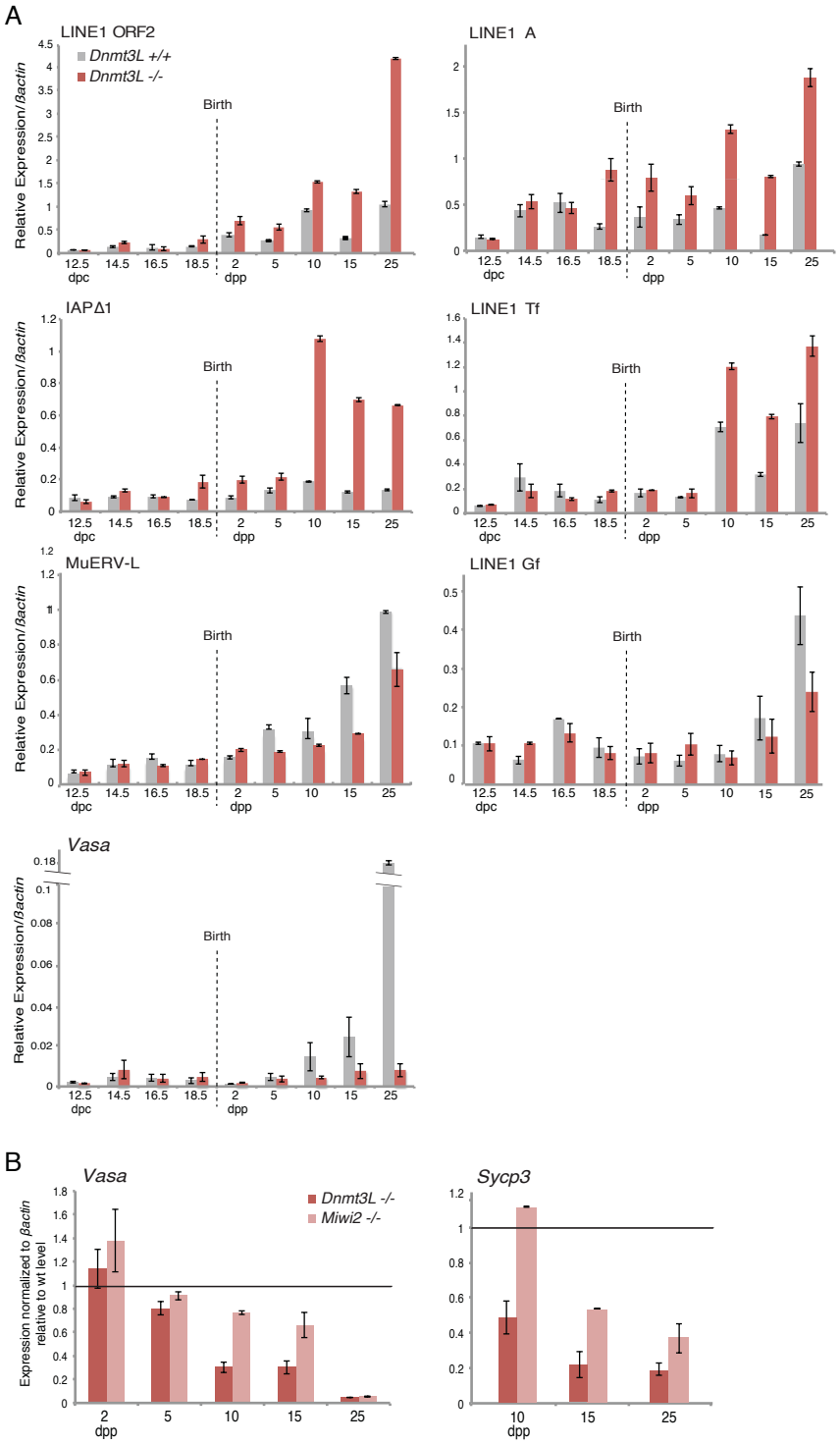
A
LINE1 ORF2
Dnmt3L +/+
Dnmt3L -/-
Relative Expression/βactin
Birth
12.5 dpc
14.5
16.5
18.5
2 dpp
5
10
15
25
LINE1 A
IAPΔ1
LINE1 Tf
MuERV-L
LINE1 Gf
Vasa
B
Vasa
Sycp3
Dnmt3L -/-
Miwi2 -/-
Expression normalized to βactin relative to wt level
2 dpp
5
10
15
25
10 dpp

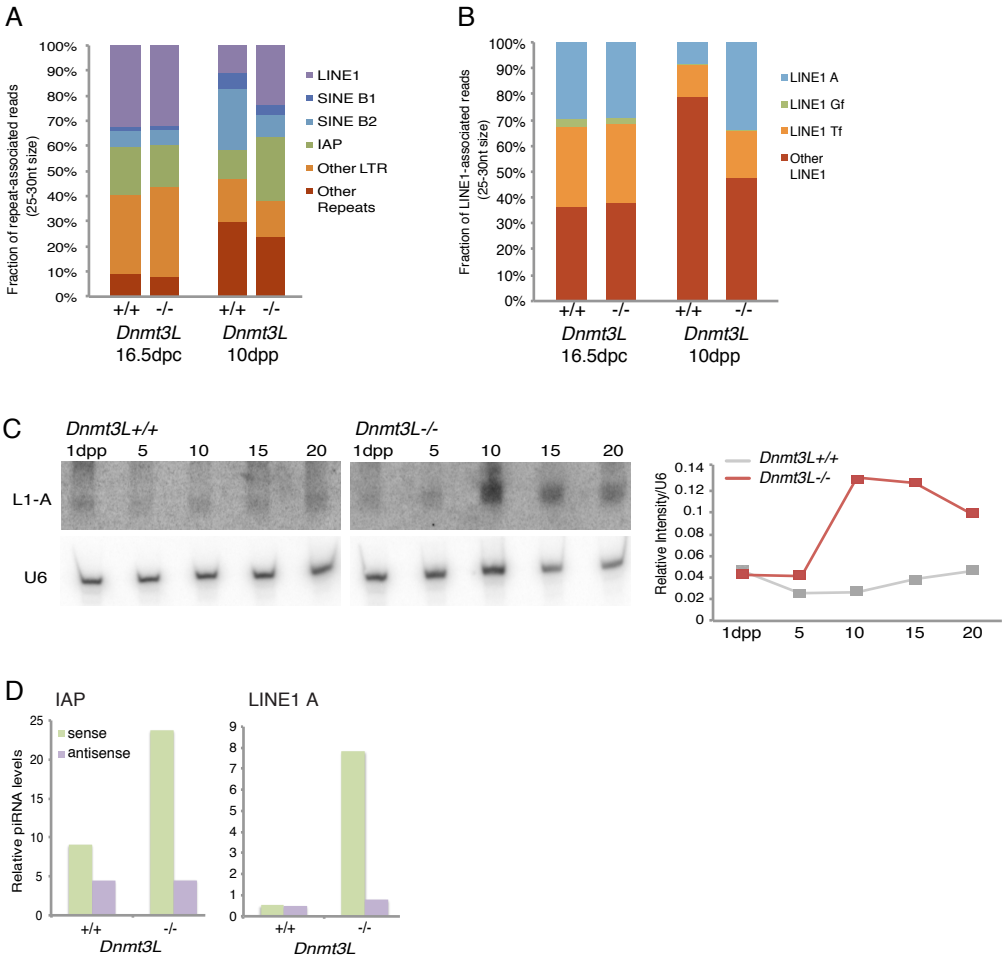
A
Fraction of repeat-associated reads (25-30nt size)
100%
90%
80%
70%
60%
50%
40%
30%
20%
10%
0%
LINE1
SINE B1
SINE B2
IAP
Other LTR
Other Repeats
+/+ -/- +/+ -/-
Dnmt3L Dnmt3L
16.5dpc 10dpp
B
Fraction of LINE1-associated reads (25-30nt size)
LINE1 A
LINE1 Gf
LINE1 Tf
Other LINE1
+/+ -/- +/+ -/-
Dnmt3L Dnmt3L
16.5dpc 10dpp
C
Dnmt3L+/+
1dpp 5 10 15 20
Dnmt3L-/-
1dpp 5 10 15 20
L1-A
U6
Dnmt3L+/+
Dnmt3L-/-
Relative Intensity/U6
0.14
0.12
0.1
0.08
0.06
0.04
0.02
0
1dpp 5 10 15 20
D
IAP
LINE1 A
Relative piRNA levels
sense
antisense
25
20
15
10
5
0
9
8
7
6
5
4
3
2
1
0
+/+ -/-
Dnmt3L
+/+ -/-
Dnmt3L

A

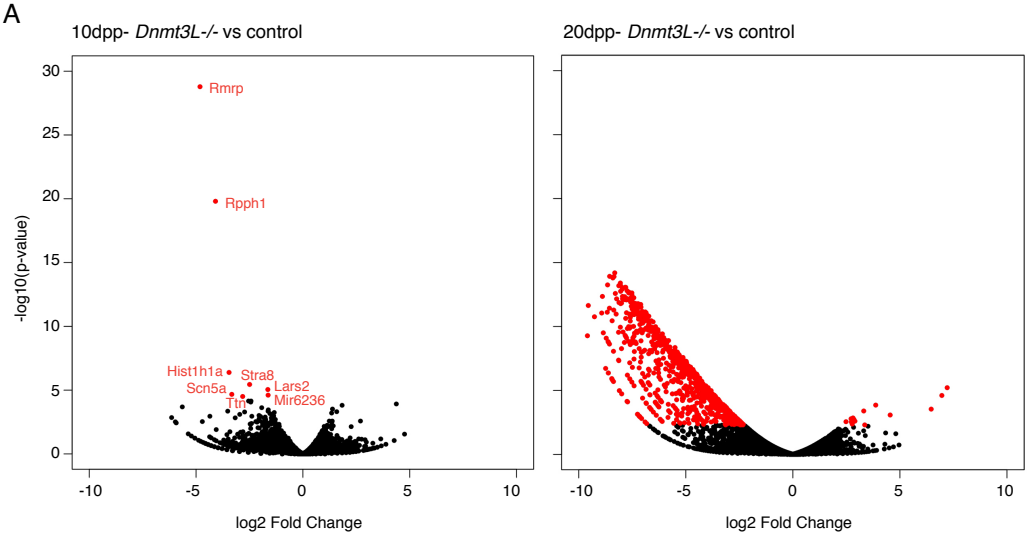
10dpp- Dnmt3L-/- vs control
20dpp- Dnmt3L-/- vs control
-log10(p-value)
log2 Fold Change
log2 Fold Change
Rmrp
Rpph1
Hist1h1a
Scn5a
Stra8
Lars2
Mir6236
Tlr1

B

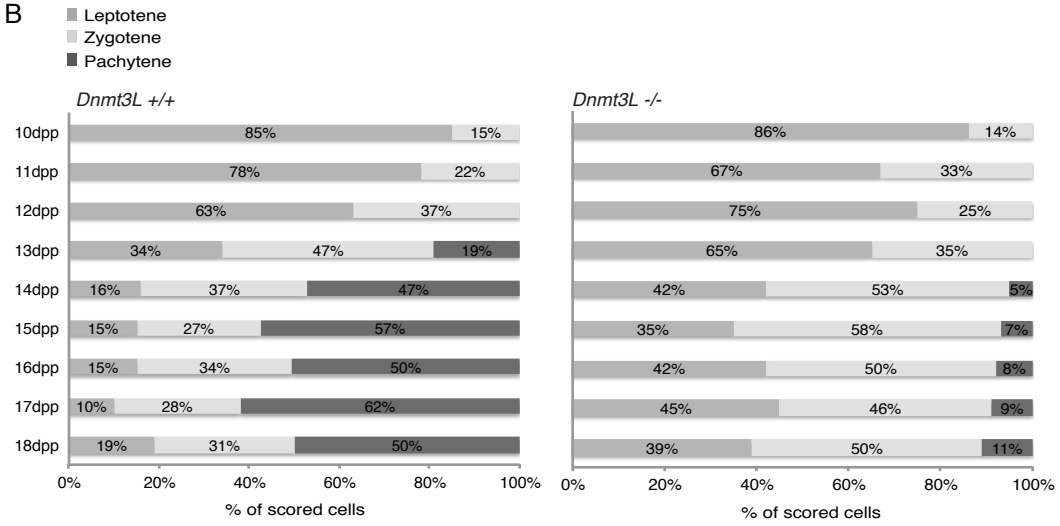
Leptotene
Zygotene
Pachytene
Dnmt3L +/+
Dnmt3L -/-
10dpp 85% 15%
11dpp 78% 22%
12dpp 63% 37%
13dpp 34% 47% 19%
14dpp 16% 37% 47%
15dpp 15% 27% 57%
16dpp 15% 34% 50%
17dpp 10% 28% 62%
18dpp 19% 31% 50%
10dpp 86% 14%
11dpp 67% 33%
12dpp 75% 25%
13dpp 65% 35%
14dpp 42% 53% 5%
15dpp 35% 58% 7%
16dpp 42% 50% 8%
17dpp 45% 46% 9%
18dpp 39% 50% 11%
0% 20% 40% 60% 80% 100%
% of scored cells
% of scored cells

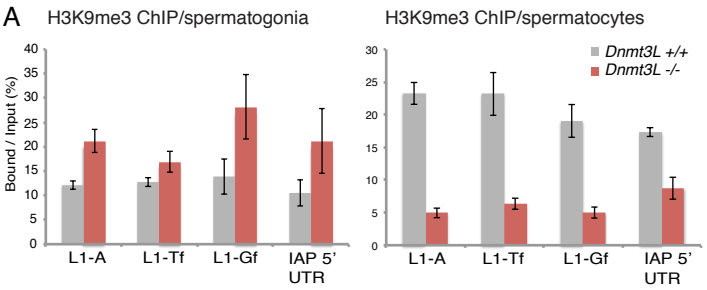
A
H3K9me3 ChIP/spermatogonia
H3K9me3 ChIP/spermatocytes
Bound / Input (%)
Dnmt3L +/+
Dnmt3L -/-
L1-A
L1-Tf
L1-Gf
IAP 5' UTR

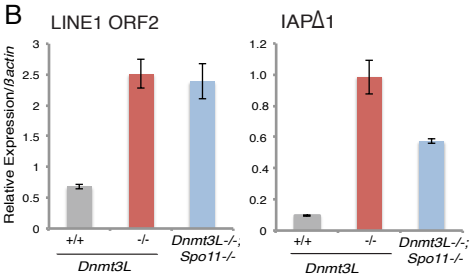
B
LINE1 ORF2
IAPΔ1
Relative Expression/βactin
+/+
-/-
Dnmt3L-/-; Spo11-/-
Dnmt3L

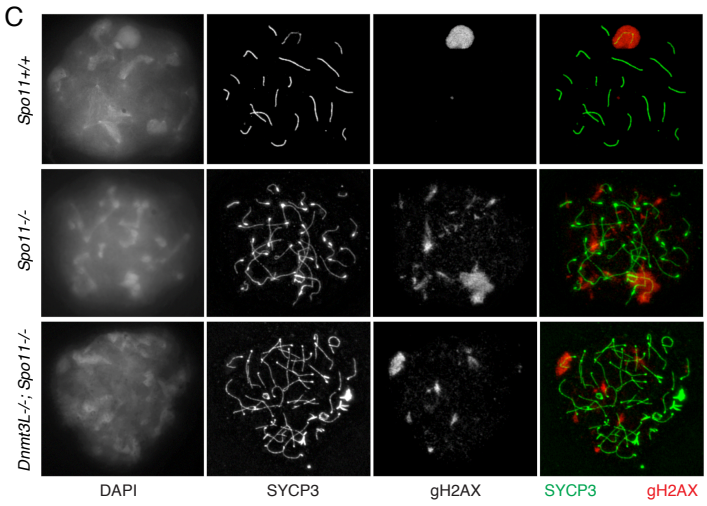
C
Spo11+/+
Spo11-/-
Dnmt3L-/-; Spo11-/-
DAPI
SYCP3
gH2AX
SYCP3
gH2AX

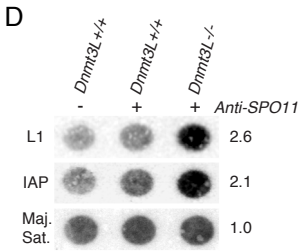
D
Dnmt3L +/+
Dnmt3L +/+
Dnmt3L -/-
-
+
+
Anti-SPO11
L1
IAP
Maj. Sat.
2.6
2.1
1.0

Supplemental Figure Legends

Supplemental Figure S1. Steady-state levels of TE and germline transcripts during normal and *Dnmt3L* mutant spermatogenesis (A) RT-qPCR analysis of TE and *Vasa* expression in prenatal (dpc) and postnatal (dpp) pooled testes from *Dnmt3L*$^{+/+}$ and *Dnmt3L*$^{-/-}$ mice. Values were normalized to *βactin.* Error bars, SEM of technical replicates. Similar results were obtained with *Rrm2* normalization. (B) RT-qPCR analysis of *Vasa* and *Sycp3* expression in postnatal pooled *Dnmt3L*$^{-/-}$ and *Miwi2*$^{-/-}$ testes relative to wt littermates. *Vasa* is a universal germ cell marker constitutively expressed in post-natal spermatogenesis, while *Sycp3* is specific to meiotic stages. The germ cell depletion in the mutant testes can be read as decreased expression of these markers.

Supplemental Figure S2. Participation of the piRNA pathway to the regulation of TEs during *Dnmt3L* mutant spermatogenesis (A) Small RNA-seq libraries from *Dnmt3L*$^{+/+}$ and *Dnmt3L*$^{-/-}$ pooled testes at 16.5dpc and 10dpp. RepeatMasker annotation of repeat-associated reads (read size 25-30nt) is indicated. LINE-1 and IAP-derived species are more abundant in *Dnmt3L*$^{-/-}$ gonads at 10dpp but not at 16.5dpc compared to wt gonads. (B) Small RNA-seq libraries from *Dnmt3L*$^{+/+}$ and *Dnmt3L*$^{-/-}$ pooled testes at 16.5dpc and 10dpp. RepeatMasker annotation of LINE1-associated reads (read size 25-30nt) is indicated. (C) Small RNA northern detection of L1-A piRNAs in postnatal testes of *Dnmt3L*$^{+/+}$ and *Dnmt3L*$^{-/-}$ mice. Loading was controlled by hybridization against U6 spliceosomal RNA. The right panel shows the relative intensity of the L1-A piRNA signal normalized to U6 plotted for each developmental timepoint. The increase in L1-A piRNA production becomes only apparent after 10dpp in *Dnmt3L*$^{-/-}$ testes. (D) Relative levels of sense and anti-sense 25-30nt small RNAs mapping to IAP and LINE1-A elements in *Dnmt3L*$^{+/+}$ and *Dnmt3L*$^{-/-}$ testes at 10dpp. The piRNA excess is mostly seen in the sense orientation, suggesting post-transcriptional cleavage of primary TE mRNAs.

Supplemental Figure S3. Gene expression and cell progression at meiosis in *Dnmt3L* mutant testes (A) Volcano plots showing changes in gene expression in *Dnmt3L*$^{-/-}$ testes versus control, at 10dpp (left panel) and 20dpp (right panel). Genes showing significant changes (p-value<0.05 and Fold Change>2) are highlighted in red, the names are indicated for the eight misregulated genes at 10dpp. (B) Distribution of *Dnmt3L*$^{+/+}$ and *Dnmt3L*$^{-/-}$ spermatocytes among different substages of meiotic prophase I, from 10 to 18dpp. Two hundred cells were scored into leptotene, zygotene and pachytene by SYCP3

immunofluorescence staining for each timepoint (two mice for each genotype and timepoint). To avoid misclassification as zygotene, mutant spermatocytes exhibiting extensive asynapsis or non-homologous synapsis were excluded from the analysis. Mutant spermatocytes were classified as pachytene only when autosomal synapsis was complete (but X and Y pairing was deficient).

Supplemental Figure S4. H3K9 methylation patterns and effects of *Spo11* deficiency in *Dnmt3L* mutant testes (A) H3K9me3 enrichment at TEs determined by ChIP-qPCR. ChIP was performed on EpCAM-expressing spermatogonia (*left panel*) and 4N spermatocytes (*right panel)* sorted from *Dnmt3L*$^{+/+}$ and *Dnmt3L*$^{-/-}$ testes. Quantitative data is expressed as the ratio of the enriched ChIP DNA (Bound) to the input DNA (Input). Error bars, SEM of two technical replicates. (B) RT-qPCR analysis shows that L1 ORF2 and IAPΔ1 are reactivated in 15dpp *Dnmt3L*$^{-/-}$*; Spo11*$^{-/-}$ testes, in levels similar to age-matched *Dnmt3L*$^{-/-}$ testes. Data were normalized to *βactin;* error bars, SEM of technical replicates. (C) Double-immunofluorescence staining of SYCP3 (green) and γH2AX (red) on spermatocytes. Accumulation of γH2AX around the partially synapsed X and Y chromosomes defines the sex body in WT (*Spo11*$^{+/+}$) spermatocytes (upper panel). In *Dnmt3L*$^{-/-}$*; Spo11*$^{-/-}$*,* mutant spermatocytes, meiotic DSB-independent pseudo-sex bodies can be seen, within the same extent of γH2AX as previously reported in *Spo11*$^{-/-}$ mutants. (D) Enrichment of SPO11 cutting sites at TE sequences. SPO11-associated single-stranded DNA fragments were immunoprecipitated from 18dpp wt and *Dnmt3L*$^{-/-}$ testis extracts. Dotted DNA was hybridized with L1-Tf and IAP-Ez full-length probes. Loading was controlled by hybridization with a major satellite DNA probe.

Supplemental Experimental Procedures

Meiotic spreads and immunofluorescence

Meiotic spreads were prepared as described previously (Barlow et al. 1997). Following fixation, slides were blocked and permeabilized with 1% horse serum, 0.3% BSA and 0.5% Triton-X for 30 minutes at room temperature. Spreads were incubated at 4°C overnight with primary antibodies listed in Supplemental Table S1. Spreads were incubated with secondary antibodies at room temperature for 1 hour, then washed in PBS followed by a brief wash in 0.4% Photoflo and air drying. For imaging, an upright epifluorescence microscope (Zeiss) was used. For counting of DMC1 foci, an inverted laser-scanning confocal microscope LSM 7000 (Zeiss) was used followed by analysis with the ImageJ image analysis and processing program.

Immunofluorescence on testis sections

Immunostaining was performed as previously described (Aravin et al. 2008), with minor modifications. Briefly, testes were fixed in 4% paraformaldehyde for 3-4 hours (prenatal testes) or overnight (postnatal testes) at 4°C. After PBS washes, pre-natal testes were transferred to 30% sucrose at 4°C; post-natal testes were transferred to 15% sucrose and then 30% sucrose at 4°C. Testes were embedded in OCT and kept at -80°C until use. Testis sections were cut at 8-10µm thickness. Before immunofluorescence, testis sections were left at room temperature for 30 minutes. Sections were blocked and permeabilized with 10% horse serum, 3% BSA and 0.2% Triton for 1 hour at room temperature. Sections were incubated with primary antibodies at 4°C overnight. For imaging, an inverted laser-scanning confocal microscope LSM 7000 (Zeiss) was used. Antibodies are described in Table S1.

Combined Immunofluorescence and RNA FISH

Preparation of male germ cells, immunofluorescence (IF) and RNA fluorescence *in situ* hybridization (RNA FISH) was performed as previously described (Namekawa and Lee 2011). Spermatocyte staging was carried out with a mouse anti-mouse SYCP3 antibody (Abcam ab12452). For L1-A detection by RNA FISH, we used a plasmid containing a 906bp region spanning the L1-A monomers of the L1Md-A3.6 element cloned into the pcR4-Topo vector (Bourc'his and Bestor 2004). The probe was labeled by nick translation (Vysis) with Spectrum Red-dUTP following manufacturer's instructions and ~50-100ng of DNA was used per slide. Before hybridization, the labeled probe was precipitated (10µg salmon testes DNA, 3M sodium acetate and 100% Ethanol), washed with 70% Ethanol and resuspended in

hybridization buffer (50% formamide, 10% Dextran, 2X SSC, 0.1% BSA, 20mM ribonucleoside-vanadyl complex). The probe was denatured at 80°C for 10 minutes and applied directly to germ cells. Hybridization was performed overnight at 37°C. For imaging and analysis of L1-A RNA localization, an epifluorescence microscope (Zeiss) was used.

Small RNA sequencing and analysis

Small-RNA seq was done using the Illumina HiSeq 2000 at Fasteris (http://www.fasteris.com, Switzerland) on libraries prepared with the Illumina TruSeq small RNA protocol from 18-35nt RNAs size-fractionated on acrylamide gel.

The trimmed sequencing reads of each small RNA-seq library were analyzed with ncPRO-seq v1.5.1 (Chen et al. 2012). Briefly, read alignment was done using Bowtie v0.12.8, allowing a sum of qualities of mismatching bases lower than 50 (-e 50); 16M to 39M mapped reads were obtained per library. The reads with up to 5,000 hits on the genome were used for transposon analysis. Aligned reads were annotated using RepeatMasker, and the positional read coverage was weighted by mapping site numbers. After exonic, microRNA and tRNA reads were removed, each read was classified as sense or antisense according to mapped strand and transcription sense of corresponding TEs.

Quantitative RT-qPCR

For prenatal samples, gonads were pooled from ~5-7 mice per genotype. For postnatal samples, testes were pooled from 3 mice per genotype. For *SCAR, Spo11, H2AX, Dmc1* and *Stra8* mutants, testes from one 6 week-old animal were used. RNA was extracted by the TRIzol method and DNase-treated (Qiagen) prior to cDNA conversion (Superscript III, Life Technologies). Quantitative amplification of cDNA was performed in triplicate using the SYBR Green technology (PCR primers listed in Table S1) on a 7900 HT Fast Real Time PCR System (Applied Biosystems).

Small RNA northern blotting

Testes were pooled from ~3-10 mice per genotype. To detect L1-A-derived piRNAs, 30µg of total testis RNA was loaded onto a 17.5% polyacrylamide/7M urea gel. Hybridization was performed as previously described (Varallyay et al. 2007) at 42°C using DNA oligonucleotide probes (Table S2). The relative intensity of L1-A piRNAs and U6 spliceosomal RNA was measured using the ImageJ analysis and processing program.

Quantification of transposon genomic copy number

Genomic DNA was isolated from three biological replicates of *Dnmt3L*$^{+/+}$ and *Dnmt3L*$^{-/-}$ FACS-sorted testis cells (2N, 4N and apoptotic, as described in the main manuscript) using the Qiagen MicroAmp kit and from wt C55Bl/6J liver, according to standard procedures. Absolute copy numbers of IAPΔ1 and L1-ORF2 were calculated by establishing standard curves plotting absolute Ct values against serial dilutions of PCR targets cloned into the pCR2.1-TOPO vector (Life Technologies). All qPCR data points were assayed in quadruplicate for three independent biological replicates on a 7900 HT Fast Real Time PCR System (primers listed in Table S2). With this set up, we estimated a copy number of 256 IAPΔ1 and 3048 L1-ORF2 fragments in wt liver DNA. These numbers were within the same range as the number of hits obtained by Blast querying the mouse genome with the same PCR primers sets (159 and 3779, respectively). The sensitivity and intra-assay variability in detecting extra-transposon copies was determined by spiking in known amounts of copies into mouse liver DNA, allowing us to distinguish 20 IAPΔ1 and 55 L1-ORF2 additional copies per mouse genome, therefore an average of 1 to 10% of copy number increase.

Supplemental References

Aravin AA, Sachidanandam R, Bourc'his D, Schaefer C, Pezic D, Toth KF, Bestor T, Hannon GJ. 2008. A piRNA pathway primed by individual transposons is linked to de novo DNA methylation in mice. *Molecular cell* 31: 785-799.

Barlow AL, Benson FE, West SC, Hulten MA. 1997. Distribution of the Rad51 recombinase in human and mouse spermatocytes. *EMBO J* 16: 5207-5215.

Bourc'his D, Bestor TH. 2004. Meiotic catastrophe and retrotransposon reactivation in male germ cells lacking Dnmt3L. *Nature* 431: 96-99.

Namekawa SH, Lee JT. 2011. Detection of nascent RNA, single-copy DNA and protein localization by immunoFISH in mouse germ cells and preimplantation embryos. *Nat Protoc* 6: 270-284.

Varallyay E, Burgyan J, Havelda Z. 2007. Detection of microRNAs by Northern blot analyses using LNA probes. *Methods* 43: 140-145.